Quasiclassical treatment of the Auger effect in slow ion-atom collisions

F. Frémont
Université de Caen, CIMAP, 6 Bd du Mal Juin, 14050 Caen Cedex, France
(Received 18 July 2017; published 18 September 2017)

A quasiclassical model based on the resolution of Hamilton equations of motion is used to get evidence for Auger electron emission following double-electron capture in 150-keV Ne^{10+} + He collisions. Electron-electron interaction is taken into account during the collision by using pure Coulombic potential. To make sure that the helium target is stable before the collision, phenomenological potentials for the electron-nucleus interactions that simulate the Heisenberg principle are included in addition to the Coulombic potential. First, single- and double-electron captures are determined and compared with previous experiments and theories. Then, integration time evolution is calculated for autoionizing and nonautoionizing double capture. In contrast with single capture, the number of electrons originating from autoionization slowly increases with integration time. A fit of the calculated cross sections by means of an exponential function indicates that the average lifetime is 4.4×10^{-3} a.u., in very good agreement with the average lifetime deduced from experiments and a classical model introduced to calculate individual angular momentum distributions. The present calculation demonstrates the ability of classical models to treat the Auger effect, which is a pure quantum effect.

DOI: 10.1103/PhysRevA.96.032712

I. INTRODUCTION

Since the pioneering work in the 1920s by Meitner [1] and Auger [2], Auger effect and autoionization, which consist of an Auger-type process involving outer levels of an atom or an ion, have been extensively studied either experimentally or theoretically and used in many fields, such as photoelectron spectroscopy [3–5] or collisions between charged particles (electron and ions) and atomic or molecular targets [6–13]. Specifically, since the beginning of the 1970s, Auger electron spectroscopy has been a powerful tool to study the process of double-electron capture (DC) in collisions between slow multiply charged ions and He atoms [7,14–24] in order to study the mechanisms responsible for electron capture.

In the simplest case of collisions involving fully stripped ions A^{Z+} and He targets, the capture processes that occur are written as follows:

$$A^{Z+} + He(1s^2) \rightarrow A^{(Z-1)+}(nl) + He^{+}, \quad (1a)$$

$$\rightarrow A^{(Z-2)+}(n\,\mathrm{ln}'\,l') + He^{2+}, \quad (1b)$$

$$\rightarrow A^{(Z-1)+}(nl) + He^{+} + e^{-}_{A}, \quad (1c)$$

$$\rightarrow A^{(Z-1)+}(nl) + He^{+} + e^{-}. \quad (1d)$$

In Eq. (1a), one He electron is captured (single capture, or SC). In Eq. (1b), both He electrons are captured onto $nln'l'$ configurations of the projectile and remain on the projectile. (n, n' and l, l' are the principal quantum numbers and angular momenta of the electrons on the projectile, respectively.) After the collision, the projectile deexcites by means of photon emission, with linewidth Γ_R. In process (1c), both electrons are also captured onto $nln'l'$ configurations of the projectile, but the projectile deexcites via autoionization, giving rise to an Auger electron e^{-}_{A}. In the last case (1d), one He electron is captured onto the projectile while the second He electron is ionized. The latter process is called transfer ionization (TI).

We focus on the DC process, which is of interest in the present work. Since collision time τ_C is of the order of 10^{-16} s at projectile energies of a few keV, and deexcitation times τ_A for autoionization and τ_R for photon emission are typically 10^{-14} and 10^{-10} s, respectively, the latter quantities are much larger than τ_C. Hence, in the first approximation, the collision can be divided in two separated steps: The first step is the collision itself, where DC occurs. The second step, also called postcollision, consists of the deexcitation of the projectile via autoionization or photon emission. In the case of autoionization, since it follows an exponential decrease of the form $e^{-\Gamma'_A}$, the electrons are emitted not only in the Coulombic field of the excited projectile, but also in that of the He^{2+} target, meaning that, in principle, both processes are not independent and cannot be separated. The need not to separate collision and postcollision processes has been demonstrated, for example, in the theoretical analysis of double excitation of D_2 following fast electron impact [25]. It has been shown that doubly excited D_2 atoms may autoionize at very short distances between both D^+ nuclei, leading to a bound D_2^+ molecular ion. In addition, at small projectile velocities (typically < 0.1 a.u.), the separation of the processes is no more valid, since $\tau_C \approx \tau_A$, especially if it is desired to differentiate between nonautoionizing double capture (NADC) and autoionizing double capture (ADC). Thus, it is clear that for many collision systems, collision and postcollision have to be theoretically treated at the same time.

Since autoionization is a pure quantum effect, quantum mechanics is the most powerful tool to treat the whole collision. As shown previously, a complete theoretical description of ion-atom collisions involving two electrons requires the use of electron correlation to account, for example, for the production of nonequivalent electron configurations $nln'l'$ ($n' \gg n$) of the projectile at low projectile energies [15,26–28]. Electron correlation was found also to be important in DC at high projectile energy [29].

However, the introduction of dynamic electron correlation in quantum-mechanical calculations remains a challenge, because the collision is, in this case, a true four-body problem. In addition, the treatment of the channels corresponding to SC and DC requires, in principle, the inclusion of a large number of basis states. Therefore, to check the validity of the model that includes electron correlation and the role of the latter interaction, couplings between the entry channel and the DC

channels, or between SC and DC channels, had to be cancelled. Despite these efforts, the ratio between experimental and theoretical cross sections could reach a factor of 2 at particular projectile energies [26].

In view of these difficulties, classical calculations have been proved to be a good alternative to analyze collision processes and determine cross sections. Classical-trajectory Monte Carlo (CTMC) methods treat the particles as classical point particles which interact through Coulomb's law with their motion as governed by Newton's law. Most of the collisions involving two electrons have been studied assuming two independent electrons, i.e., neglecting electron correlation [30–33]. The agreement between experiment and calculations was found to be reasonable for total cross sections at projectile velocities larger than the target electron classical velocity.

To incorporate electron correlation in the collision, several methods have been introduced [34–37] to deal with the multielectron problem. In some cases electron-electron interaction is given by the sum of Coulombic potential $1/\|\overrightarrow{r_1} - \overrightarrow{r_2}\|$ ($\overrightarrow{r_1}$ and $\overrightarrow{r_2}$ are the position vectors of both electrons in the laboratory frame) and phenomenological potentials to insure the stability of He (otherwise, the He atom would spontaneously autoionize) [34,35]. In contrast, other theories [36,37] only partially take into account electron correlation by means of a dynamic screening of the target nucleus as seen by each of the two active electrons.

The question arises if it is possible or not to classically describe and quantify autoionization in ion-atom collisions, since it is a pure quantum effect, and since ADC and TI processes give rise to the same final states. However, at low projectile energies, it is well known that TI cross sections σ_{TI} are much smaller than ADC cross sections σ_{ADC}, since ionization probability is smaller than capture probability. Therefore, if one electron from He is captured while the other one is ionized at the end of the collision, it seems reasonable to conclude that the process involved in this final state is ADC.

To characterize in more detail the latter process, a time dependence of the probability for autoionization can be achieved and compared with the time dependence of probability for other processes, i.e., NADC, single ionization (SI), or SC. Since the cross section σ_P for process P is defined at infinity, we introduce an intermediate quantity $\tilde{\sigma}_P$, whose dimension is the same as that of a cross section. This quantity is defined as $\tilde{\sigma}_P = \int_0^{b_{\max}} 2\pi\, b\, P(b,t_c)\, db$, where b is the impact parameter, $b_{\max}$ is the maximum value of b, and $P(b,t_c)$ is the probability for the process P to occur after a collision time equal to t_c. At infinity, $\tilde{\sigma}_P$ tends towards σ_P.

Figure 1 shows a schematic expected behavior of $\tilde{\sigma}_{\mathrm{ADC}}$ (full curve), $\tilde{\sigma}_{\mathrm{NADC}}$ (dashed curve), and $\tilde{\sigma}_{\mathrm{SC}} + \tilde{\sigma}_{\mathrm{SI}}$ (dotted-dashed curve) as a function of time. (Here $t = 0$ corresponds to the time at which the projectile and the target are in the (xOy) plane, perpendicular to the (Oz) axis, representing the direction of the projectile before the collision.)

During the collision, i.e., between $-t_o$ and t_o, the two nuclei and the electrons constitute a quasimolecule (illustrated by a short-dashed Gaussian curve) so that both electron energies in the projectile and target frames are negative. Let us suppose that at a time close to t_o, N_{DC}^{O} are captured by the projectile, giving rise to $\tilde{\sigma}_{\mathrm{ADC}}$. The latter quantity

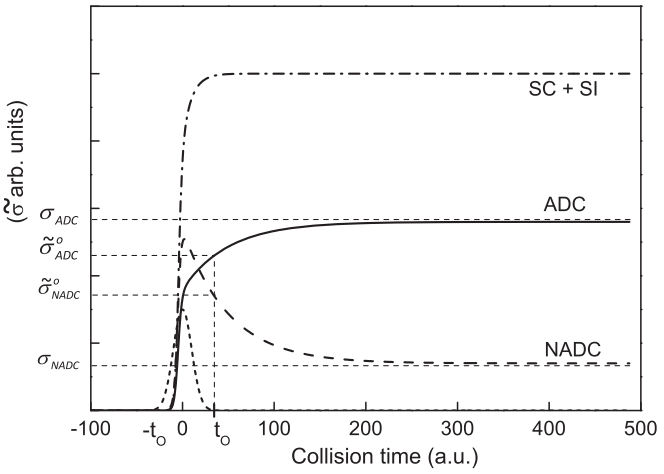

FIG. 1. Schematic expected behavior of $\tilde{\sigma}_{\mathrm{ADC}}$ (full curve), $\tilde{\sigma}_{\mathrm{NADC}}$ (dashed curve), and $\tilde{\sigma}_{\mathrm{SC}} + \tilde{\sigma}_{\mathrm{SI}}$ (dotted-dashed curve) as a function of integration time t. The short-dashed curve shows the time interval during which the quasimolecule is formed. In this interval, the electrons are shared between both nuclei.

decreases with time, reaching the value σ_{NADC} at the end of the collision (dashed curve in Fig. 1). In contrast, the quantity $\tilde{\sigma}_{\mathrm{ADC}}$ increases slowly with time. Since the number of events is conserved, the relation $\tilde{\sigma}_{\mathrm{ADC}} + \tilde{\sigma}_{\mathrm{NADC}} = \sigma_{\mathrm{ADC}} + \sigma_{\mathrm{NADC}}$ has to be verified. On the other hand, since SC and SI occur during the collision, i.e., in the range from $-t_o$ to t_o, approximately, the number of involved electrons is expected to be constant at $t > t_o$. This schematic comparison clearly shows that it is possible, in principle, to find a signature of autoionization by analyzing the collision at various integration times. Indeed, by fitting the calculated cross sections with a formula of the type

$$a_o + b_o \exp(-\Gamma t), \tag{2}$$

where a_o and b_o are adjustable parameters and Γ is a quantity that represents an average width, it is expected that widths Γ_{SC} and Γ_{SI} for SC and SI, respectively, are much larger than Γ_{NADC} and Γ_{ADC} for NADC and ADC, respectively.

In the present work, we focus on the particular case of $Ne^{10+} + He$ collisions at a projectile energy of 150 keV, which has been extensively studied experimentally and theoretically [18,26,27,38]. This energy corresponds to a velocity of ∼0.53 a.u., which is smaller than the classical velocity of the He electron (∼1.3 a.u.). Therefore, at 150 keV, total cross sections calculated using CTMC model are expected to deviate from experiment. However, this point is not crucial, since we are interested in the average width Γ rather than cross sections.

The method to calculate calculations cross sections is summarized in Sec. II. Differential and total SC and DC capture cross sections are then deduced and compared with previous values. Particular attention is devoted to the dependence of cross sections with integration time. In order to get clear evidence for autoionization, this dependence is compared with that formed when electron correlation is not included in the calculation. Finally, from our results, an autoionization width $\overline{\Gamma_A}$ is evaluated and compared with that estimated from previous calculations and experimental cross sections [38].

In the following, the independent-electron CTMC model and correlated-electron CTMC model will be referred as IE-CTMC and CE-CTMC models, respectively.

II. DESCRIPTION OF CTMC METHOD

The CTMC method is based on a numerical solution of Hamilton's equations of motion for the many-body system, which includes the Ne^{10+} and He^{2+} nuclei, as well as both He electrons. The general expression of the classical Hamiltonian reads

$$H = \sum_{k=1}^{4} \frac{p_k^2}{m_k} + \sum_{k=1}^{3} \sum_{j=k+1}^{4} \frac{q_j q_k}{r_{jk}} + \sum_{i=1}^{2} \sum_{\beta=1}^{2} V_H^{\beta}(r_{\beta i} p_{\beta i}). \quad (3)$$

In the above expression, $\overrightarrow{p_k}$, q_k, and m_k are the momentum vector, and the charge and the mass of particle k, respectively. The quantity r_{jk} is the distance between particles j and k. The pseudopotential $V_H^{\beta}(r_{\beta i} p_{\beta i})$, where β denotes each nucleus and i the index for each electron, was first introduced in nuclear physics [39] and then adapted for atom structures [40] and ion-atom [41,42] or ion molecule collisions [43]. Its expression is

$$V_H^{\beta} = \frac{\xi_H^2}{4\alpha \mu_{\beta} r_{\beta i}^2} \exp\left\{\alpha\left[1 - \left(\frac{r_{\beta i} p_{\beta i}}{\xi_H}\right)^4\right]\right\}. \quad (4)$$

In this relation, μ_{β} is the reduced mass between each nucleus and one He electron. The quantities $\xi_H = 0.9582$ and $\alpha = 4$ were chosen so that the first and second ionization potentials of He are close to experimental ones [43]. With these values, first and second ionization potentials of He are 1.1 and 2.3 a.u., respectively, which is consistent with the expected values of 0.9 and 2 a.u. The quantities $r_{\beta i}$ and $p_{\beta i}$ are the positions and momenta of He electrons, respectively, relative to the He nucleus or the Ne nucleus.

Initially, the projectile is at a distance $z_p = -200$ a.u., and the orientation of the electron around the target is randomly chosen. The only initial constraints that insure the stability of the He atom are $\vec{r}_{\mathrm{He1}} = -\vec{r}_{\mathrm{He2}}$, and $\vec{p}_{\mathrm{He1}} = -\vec{p}_{\mathrm{He2}}$ [43]. The impact parameter b varies from 0 to 20 a.u., and the angle φ_p, which characterizes the position of the projectile in the (xOy) plane, is also randomly chosen. The initial spatial and momentum distributions were calculated using the method initiated previously by Abrines and Percival [44], developed in several cases for H target or multielectron targets (see, for example, Ref. [45]).

From the initial conditions, the Hamiltonian equations are numerically solved using the Runge-Kutta method of order 4, with an adaptive step defined and described in Ref. [44]. At the end of the collision, the number of projectiles that have captured one or two target electrons is determined as a function of the scattering angle θ_P, b and electron energy. To obtain good statistics, the number of calculated trajectories was fixed to 200 000.

When an independent model is used, the electron-electron interaction term and the pseudopotential $V_H^{\beta}(r_{\beta i} p_{\beta i})$ are cancelled. The charge of He is replaced by an effective charge of 1.704. With this value, the total electron binding energy on He is 2.904 a.u. In both cases, SC, NADC, ADC, SI, and TI processes are identified (Table I) through the sign of the energies E_i^{Ne} and E_i^{He} of each electron ($i = 1,2$) in the projectile and target referential frames, respectively.

TABLE I. Energy signs of electrons 1 and 2, in the Ne and He referential frames, for single capture (SC), double capture (DC), single ionization (SI), and autoionizing double capture + transfer ionization (ADC + TI) processes.

	E_1^{Ne}	E_1^{He}	E_2^{Ne}	E_2^{He}
SC	<0	>0	>0	<0
	>0	<0	<0	>0
NADC	<0	>0	<0	>0
SI	>0	>0	<0	<0
	<0	<0	>0	>0
ADC + TI	<0	>0	>0	>0
	>0	>0	<0	>0

III. DIFFERENTIAL AND TOTAL CROSS SECTIONS

A. Differential cross sections

Figures 2 and 3 represent differential cross sections for SC and DC, respectively, as a function of the scattering angle θ_d of the projectile. Our theoretical results (dotted-dashed curve and full curve for IE-CTMC and CE-CTMC models, respectively) are compared with previous experiments (full squares) and quantum calculations (dashed curve) [27]. Note that CTMC calculations have been normalized to experiment at the maximum of intensity.

In the case of SC, the experimental and theoretical maxima are located at about 0.07 mrd. Another maximum is observed experimentally at ∼0.13 mrd. Theoretically, a second maximum also appears, at larger angles (∼0.2 mrd for quantum and CTMC results). When the IE-CTMC model is used, the

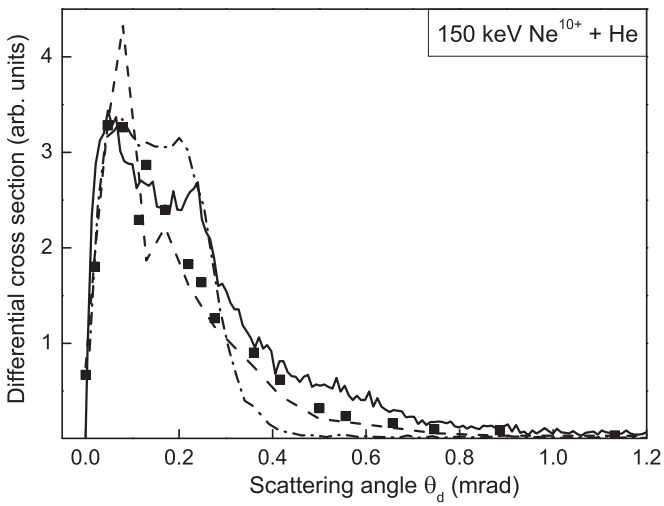

FIG. 2. Differential single capture cross sections as a function of the scattering angle of the projectile, in 150-keV Ne^{10+} + He collisions. Present theoretical results, dotted-dashed curve and full line, using an independent and correlated CTMC model, respectively; experiment, full squares; quantum calculations, dashed curves.

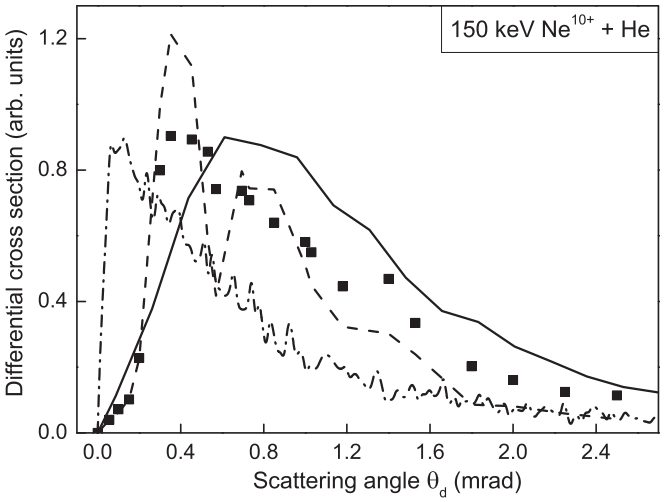

FIG. 3. Differential double capture cross sections as a function of the scattering angle of the projectile in 150-keV $Ne^{10+} + He$ collisions. Present theoretical results, dotted-dashed curve and full line, using independent and correlated CTMC model, respectively; experiment, full squares; quantum calculations, dashed curves.

distribution cancels when $\theta_d > 0.5$ mrd, while it cancels for $\theta_d > 0.8$ mrd when electron correlation is taken into account, in good agreement with experiment and quantum calculations. Moreover, the shape of the distribution is much better when electron correlation is introduced.

For DC (Fig. 3), while quantum calculations reproduce very well the experiment, the agreement between CTMC calculations and experiment is worse than for SC. However, as in the case of SC, the shape of the DC distribution is better for the CE-CTMC model than that for the IE-CTMC model. These preliminary results clearly underscore the important role of electron correlation, even in single electron processes.

B. Total cross sections

Since no result is available for single and double ionization, we concentrate only on SC, DC, and ADC. Total cross sections are calculated by integration of differential cross sections $2\pi b P(b)$, where b is the impact parameter and $P(b)$ the probability for each process. The results are summarized in Table II and compared with previous experiments and calculations [26,27,46,47]. With correlated electrons, the CTMC cross section for SC is smaller than other theories and experiment by a factor ranging from 1.6 up to 2.6. The total DC cross section, i.e., including NADC and (ADC + TI), is larger than experiment and semiclassical theory by a factor of ∼2. Surprisingly, the ADC cross section calculated by the CE-CTMC model is equal to the experimental one [26] but twice larger than the theoretical one [27]. As mentioned in the Introduction, since autoionization is not possible when both electrons are treated independently, the (ADC + TI) cross section falls down by 2 orders of magnitude. This result shows that the value we obtain with the IE-CTMC model is due to TI, while ADC is dominant when electron correlation is taken into account.

TABLE II. Cross section for SC, DC, ADC + TI in 150-keV $Ne^{10+} + He$ collisions. Exp, Ref. [46] for SC and [26] for DC. First two columns present results using IE-CTMC and CE-CTMC models, and theory for SC [47] and DC [27], last column.

	σ (10^{-16} cm^2)			
Processes	IE-CTMC	CE-CTMC	Exp	Theory
SC	15	9.5	25	20.8
NADC	5.4	5.6	1.5 ± 0.3	2.8
ADC + TI	0.12	2.6	2.6 ± 0.5	1.2

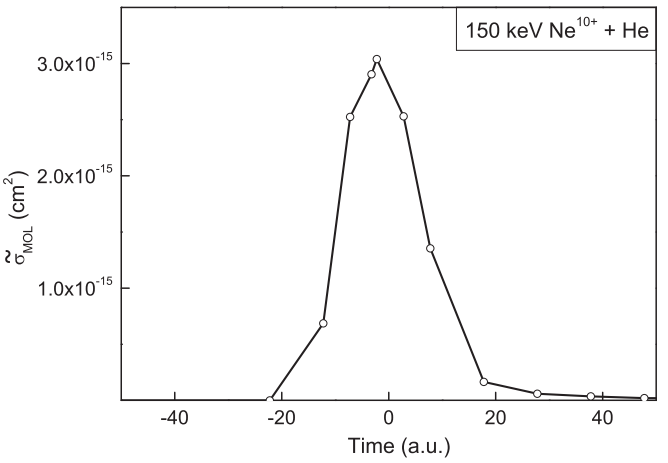

FIG. 4. Quantity $\tilde{\sigma}_{mol}$ for producing a quasimolecule $(Ne{-}He)^{8+}$. Between $-t_o$ and t_o both electrons are bound on Ne and He.

There are several reasons for explaining the differences observed between the present results, experiment [26,46] and semiclassical theory [27,47]. First, one has to recall that CTMC calculations are valid at intermediate and high energies (cf. Introduction). Second, the results depend strongly on the α parameter and, to a less extent, the initial radial and momentum electron distributions. Despite these limitations, our results using the CE-CTMC model are satisfactory.

IV. TIME EVOLUTION OF PROCESS PROBABILITIES

A. Formation of the quasimolecule

Figure 4 shows the quantity $\tilde{\sigma}_{mol}$ for producing a quasimolecule $(Ne{-}He)^{8+}$. In this configuration, both electrons are bound on Ne and He. The distribution is centered at $t = 0$ and extends to ∼40 a.u., which corresponds to a maximum internuclear distance of ∼10 a.u. This value is close to the value of 8 a.u. found for the crossing radius where SC and DC processes mainly occur [27].

B. SC and SI processes

In Figs. 5(a) and 5(b) are represented the results of the present calculations for time evolution of $\tilde{\sigma}_{SI}$ and $\tilde{\sigma}_{SC}$, respectively, from $t = 0$ to 1600 a.u. In the insets, a zoom of the evolution is shown for times smaller than 160 a.u. These quantities are found to remain constant after integration times larger than 50 a.u., within the uncertainties, meaning that SC and SI processes occur during the collision, i.e., when the four bodies form a quasimolecule. A fit of calculated cross

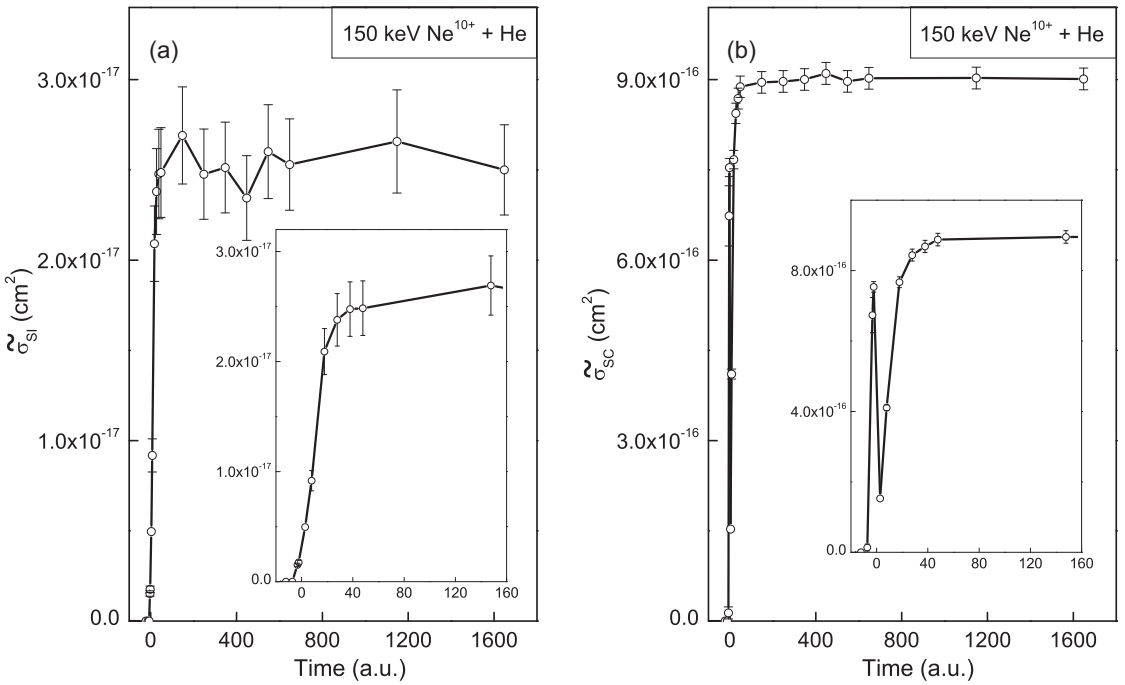

FIG. 5. Results of the present calculations for time evolution of quantities $\tilde{\sigma}_{SI}$ (a) and $\tilde{\sigma}_{SC}$ (b), from $t = 0-1600$ a.u., in 150-keV Ne^{10+} + He collisions. Inset: Zoom of time evolution for integration times smaller than 160 a.u.

sections using relation (2) gives rise to $\Gamma_{SC} = 0.10 \pm 0.05$ a.u. and $\Gamma_{SI} = 0.063 \pm 0.007$ a.u. For SC, a peak is observed at ~ -2 a.u. This peak qualitatively illustrates that one electron can be bound, during the collision, either on Ne or on He. A more detailed analysis would reveal more peaks, indicating the number of swaps an electron experiences between the projectile and target nuclei.

C. NADC and ADC processes

Figure 6 shows the time evolution of $\tilde{\sigma}_{ADC} + \tilde{\sigma}_{TI}$ (top of Fig. 6), $\tilde{\sigma}_{NADC}$ (middle of Fig. 6), and the sum of these cross sections (bottom of Fig. 6) using CE-CTMC model. In contrast with SI and SC, $\tilde{\sigma}_{NADC}$ decreases with time, to the advantage of $\tilde{\sigma}_{ADC} + \tilde{\sigma}_{TI}$, since the sum remains constant after about 50 a.u. We focus now on the $\tilde{\sigma}_{ADC} + \tilde{\sigma}_{TI}$ time evolution. Since SC and SI occur at small internuclear distances and since the probability for TI can be considered as the product of SC and SI probabilities, $\tilde{\sigma}_{TI}$ is expected to be constant after a few a.u. Hence, the shape of the time evolution observed on top of Fig. 6 is mainly due to ADC. In addition, as seen in Fig. 7, $\tilde{\sigma}_{TI}$ calculated by means of IE-CTMC is a factor of at least 10 smaller than ADC cross sections, suggesting that, at 150 keV, the time evolution of the capture and electron emission cross section is essentially caused by autoionization after the double capture process.

V. AVERAGE AUTOIONIZATION WIDTH

From calculations performed for NADC and ADC (see previous section), an average autoionization width can be evaluated by fitting $\tilde{\sigma}_{ADC}$ and $\tilde{\sigma}_{NADC}$ using an exponential function given by relation (2). The results for the parameters a_o, b_o, and Γ are summarized in Table III.

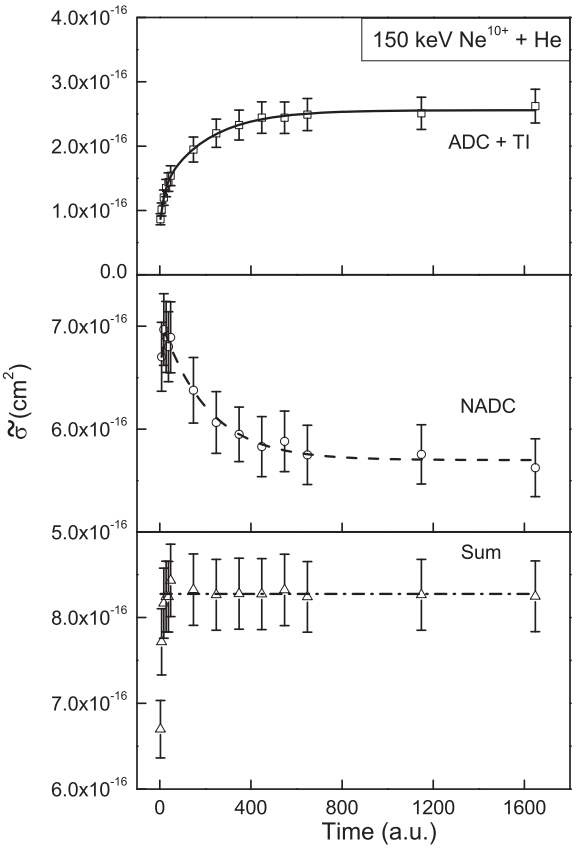

FIG. 6. Time evolution of $\tilde{\sigma}_{ADC} + \tilde{\sigma}_{TI}$ (top of Fig. 6), $\tilde{\sigma}_{NADC}$ (middle of Fig. 6), and the sum of these quantities (bottom of Fig. 6) using CE-CTMC model. For ADC + TI and NADC, a fit using relation (2) has been performed (full line on top and dashed line for NADC) in order to determine an average autoionization width.

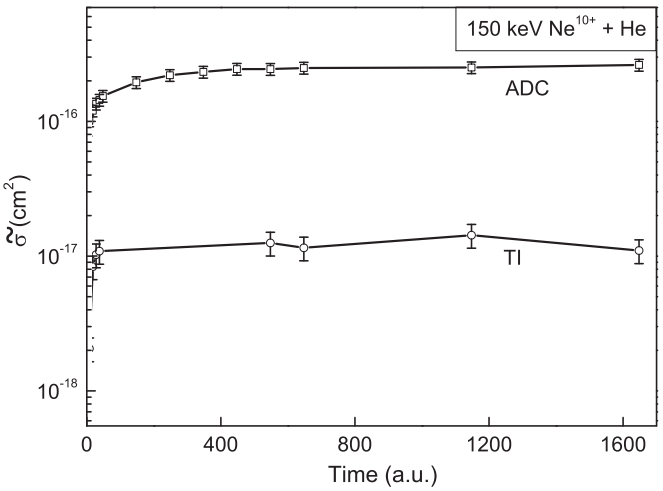

FIG. 7. Comparison between $\tilde{\sigma}_{\mathrm{ADC}}$ (empty squares) and $\tilde{\sigma}_{\mathrm{TI}}$ (empty circles) as a function of time using an independent-electron classical model.

The average autoionization width for NADC and ADC are close to each other, within the uncertainties. To verify the coherence of these values, an average autoionization width $\overline{\Gamma_A}$ has been evaluated from experimental cross sections and previous calculations of individual widths [19,26,38].

The average width $\overline{\Gamma_A}$ is given by

$$\overline{\Gamma_A} = \frac{\sum_{l,l',n,n',L} \Gamma^A_{nln'l'^1L} \sigma^A_{nln'l'^1L}}{\sum_{l,l',n,n',L} \sigma^A_{nln'l'}}. \tag{5}$$

In this expression, $\Gamma^A_{nln'l'^1L}$ is the individual width for a given term $nln'l'^1L$, where n and n' are the principal quantum numbers of the populated term, l and l' are the associated angular momenta, and L is the total angular momentum. Each value has been calculated previously and tabulated for $3lnl'$ ($n = 4$–9) and $4lnl'$ ($n = 4$–6) configurations [19,38]. The quantities $\sigma^A_{nln'l'^1L}$ are the cross sections for Auger emission after double capture onto a given $nln'l'^1L$ term. The problem is that individual cross sections $\sigma^A_{nln'l'^1L}$ are unknown, either experimentally or theoretically. To evaluate $\sigma^A_{nln'l'^1L}$, the method developed by Burgdörfer and collaborators [48] for SC in collisions between highly charged ions and an H target, based on the well-known classical over-barrier model (COBM) [49], has been used. Extending the model to DC and assuming that the target electrons are captured independently from each other, the capture cross section $\sigma_{nln'l'^1L}$ on an individual term $nln'l'^1L$ is written

$$\sigma_{nln'l'^1L} = \frac{c(l,l')}{\Delta l\, \Delta l'} \int_0^{R_C} P_l(b)\, P_{l'}(b) b db. \tag{6}$$

In this expression, $c(l,l')$ is calculated to normalize the quantity $\int_0^{R_C} P_l(b)\, P_{l'}(b) d(vb)$ (v is the projectile velocity). The quantities Δl and $\Delta l'$ are the widths of the angular momentum distributions, and $P_l(b)$ and $P_{l'}(b)$ are the individual capture probabilities on specific nl and $n'l'$ configurations, respectively, that depend on impact parameter b. Each probability is given by a Gaussian [48]:

$$P_l(b) = \frac{1}{\sqrt{\pi\, \Delta l}} \left\{ \exp\left[-\left(\frac{l + 1/2 - vb}{\Delta l} \right)^2 \right] + \exp\left[-\left(\frac{l + 1/2 + vb}{\Delta l} \right)^2 \right] \right\}. \tag{7}$$

The sum $\sigma_{nn'} = \sum_{l,l',L} \sigma_{nln'l'^1L}$ is normalized to the total experimental cross section given in Ref. [26]. Figure 8 shows the result of L distribution calculations using the present model (full squares) for configurations $3lnl'$ ($n = 3$, 6, and 9). As seen in the figure, the distributions can be approximately fitted using Gaussian curves. The maximum of the distributions is centered at ~2 and the width for each distribution is of the order of 2.5. From the l and l' distributions, each value of $\sigma_{nln'l'^1L}$ could be evaluated. Then, an individual Auger cross section $\sigma^A_{nln'l'^1L}$ could be obtained using the relation $\sigma^A_{nln'l'^1L} = \Gamma^A_{nln'l'^1L}$ $\sigma_{nln'l'^1L}$. Finally, using relation (5), $\overline{\Gamma_A}$ was deduced.

Table IV summarizes the values for $\sum_{l,l',L} \Gamma^A_{nln'l'^1L} \sigma^A_{l,l',L}$ and $\sum_{l,l',L} \sigma^A_{nln'l'^1L}$ for $3lnl'$ ($n = 4$–9) and $4lnl'$ ($n = 4$, 5)

TABLE III. Parameters a_o, b_o and $1/\Gamma$ derived from relation (3) for ADC and NADC processes.

Processes	a_o (10^{-16})	b_o (10^{-16})	Γ (a.u.)
ADC	2.64 ± 0.08	-1.65 ± 0.07	$(4.9 \pm 0.4)\ 10^{-3}$
NADC	5.70 ± 0.04	1.30 ± 0.09	$(4.3 \pm 0.7)\ 10^{-3}$

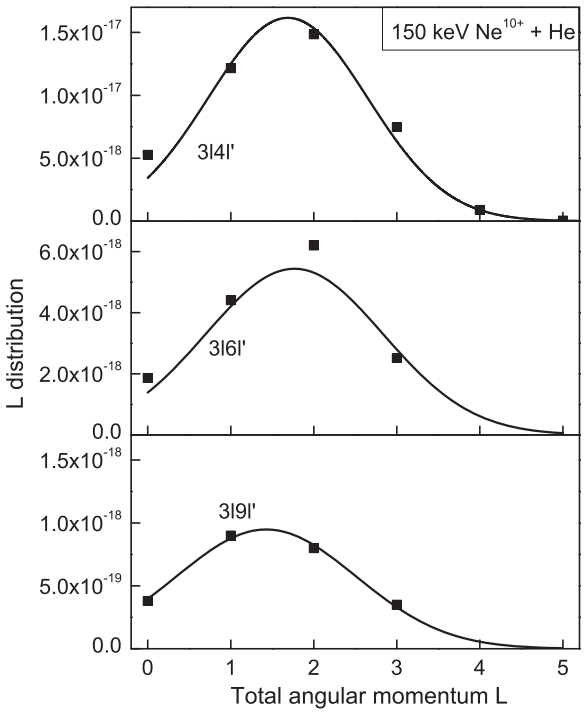

FIG. 8. L distributions of $3lnl'$ ($n = 4$, 6, and 9) configurations of Ne^{8+} (full squares), determined using a classical model developed for SC [48]. The sum of each L distribution is normalized to experimental DC cross sections [26].

TABLE IV. Values $\sum_{l,l',L} \Gamma^A_{nln'l'^1L}\sigma^A_{l,l',L}$ and $\sum_{l,l',L} \sigma^A_{nln'l'^1L}$ in cm^2 (divided by 10^{-17}) evaluated using calculated data for individual widths [19,38] and COBM [48].

Configurations	$3l4l'$	$3l5l'$	$3l6l'$	$3l7l'$	$3l8l'$	$3l9l'$	$4l4l'$	$4l5l'$
$\sum_{l,l',L} \Gamma^A_{nln'l'^1L}\sigma^A_{l,l',L}$	1.7×10^{-2}	7.2×10^{-3}	1.1×10^{-3}	7.5×10^{-4}	2.8×10^{-4}	1.2×10^{-4}	4.0×10^{-2}	3.4×10^{-2}
$\sum_{l,l',L} \sigma^A_{nln'l'^1L}$	4.07	3.93	2.3	1.5	0.8	0.5	4.4	5.0

configurations [26]. Thus, the value for $\overline{\Gamma_A}$ is $\sim 4.4 \times 10^{-3}$, which is surprisingly in very good agreement with the results of CTMC calculations, considering all the approximations that were made in the evaluation of $\overline{\Gamma_A}$.

This agreement clearly shows that the Auger effect or autoionization can be classically described without any ambiguity to describe double capture. In addition, CTMC calculations, including electron correlation, also show that configurations of nonequivalent electrons $3lnl'$ ($n > 5$) are populated. Indeed, if the contributions (Table III) of these configurations are neglected, the value for $\overline{\Gamma_A}$ is $\sim 5.6 \times 10^{-3}$, which is larger than the previous one by 25%. More detailed work on electron energy distributions would be desirable to confirm the presence of such configurations in the present calculation.

VI. CONCLUSION

A four-body classical model has been developed and applied to get evidence for the Auger effect in $Ne^{10+} + He$ collisions at a projectile energy of 150 keV. First, total SC and DC cross sections were determined and compared with previous experiments [26,46] and theories [27,47]. Then, time evolution of quantities $\tilde{\sigma}_{SI}$ and $\tilde{\sigma}_{SC}$ were calculated. These quantities were found to be constant after integration time of $\sim$50 a.u., while $\tilde{\sigma}_{ADC}$ (resp. $\tilde{\sigma}_{NADC}$) were shown to slowly increase (resp. decrease) with integration time. By fitting the time evolution of $\tilde{\sigma}_{NADC}$ and $\tilde{\sigma}_{ADC}$, an average lifetime was found to be $\sim 4.6 \times 10^{-3}$ a.u., in very good agreement with the value of 4.4×10^{-3} a.u. determined using a model preformed previously [48,49] for SC and extended to DC, assuming independent electrons.

The present result confirms the ability of a classical model to extract Auger emission cross sections following DC. This promising result is a first step in the analysis of more complicated collisions. First, the integration time dependence of the cross section can be used to study the evolution of $\overline{\Gamma_A}$ with projectile velocity. Indeed, in the case of $Ne^{10+} + He$ collisions, for example, it is well known that $3lnl'$ ($n > 5$) configurations are mainly populated when projectile velocity decreases. We thus expect a decrease of $\overline{\Gamma_A}$ with velocity.

In addition, this important result will be useful to study interferences in $He^{2+} + H_2$ collisions [50,51]. So far, theoretical studies concern only postcollision, i.e., the interaction of the two protons and the Auger electron after DC. The whole collision, including the DC process and autoionization, can now be analyzed.

[1] L. Meitner, Z. Phys. **17**, 54 (1923).
[2] P. Auger, C. R. Acad. Sci. Paris **177**, 169 (1923); **180**, 65 (1925).
[3] R. Fromherz, G. Ganteför, and A. A. Shvartsburg, Phys. Rev. Lett. **89**, 083001 (2002).
[4] T. Osipov, M. Stener, A. Belkacem, M. Schöffler, T. Weber, L. Schmidt, A. Landers, M. H. Prior, R. Dörner, and C. L. Cocke, Phys. Rev. A **81**, 033429 (2010).
[5] S.-B. Cheng, C. L. Harmon, H. Yang, and A. W. Castleman, Jr., Phys. Rev. A **94**, 062506 (2016).
[6] B. Cleff and W. Mehlhorn, J. Phys. B: At. Mol. Phys. **7**, 593 (1974).
[7] N. Stolterfoht, C. C. Havener, R. A. Phaneuf, J. K. Swenson, S. M. Shafroth, and F. W. Meyer, Phys. Rev. Lett. **57**, 74 (1986).
[8] F. Frémont, A. Hajaji, A. Naja, C. Leclercq, J. Soret, J. A. Tanis, B. Sulik, and J.-Y. Chesnel, Phys. Rev. A **72**, 050704(R) (2005).
[9] F. Frémont, A. Hajaji, J.-Y. Chesnel, P. Leprince, F. Porée, B. Gervais, and D. Hennecart, Phys. Rev. A **74**, 012717 (2006).
[10] M. Takahashi, Y. Miyake, N. Watanabe, Y. Udagawa, Y. Sakai, and T. Mukoyama, Phys. Rev. Lett. **98**, 013201 (2007).
[11] M. Fogle, D. Wulf, K. Morgan, D. McCammon, D. G. Seely, I. N. Draganić, and C. C. Havener, Phys. Rev. A **89**, 042705 (2014).
[12] R. T. Zhang, W. T. Feng, X. L. Zhu, S. F. Zhang, D. L. Guo, Y. Gao, D. B. Qian, S. Xu, S. C. Yan, P. Zhang, Z. K. Huang, H. B. Wang, B. Hai, D. M. Zhao, and X. Ma, Phys. Rev. A **93**, 032709 (2016).
[13] Å. Larson, S. M. Nkambule, and A. E. Orel, Phys. Rev. A **94**, 022709 (2016).
[14] D. H. Crandall, R. E. Olson, E. J. Shipsey, and J. C. Browne, Phys. Rev. Lett. **36**, 858 (1976).
[15] C. Harel, H. Jouin, and B. Pons, J. Phys. B: At. Mol. Phys. **24**, L425 (1991).
[16] Z. Chen and C. D. Lin, J. Phys. B: At. Mol. Phys. **26**, 957 (1993).
[17] S. Martin, A. Denis, A. Delon, J. Désesquelles, and Y. Ouerdane, Phys. Rev. A **48**, 1171 (1993).
[18] F. Fremont, H. Merabet, J. Y. Chesnel, X. Husson, A. Lepoutre, D. Lecler, G. Rieger, and N. Stolterfoht, Phys. Rev. A **50**, 3117 (1994).
[19] H. W. van der Hart, N. Vaeck, and J. E. Hansen, J. Phys. B: At. Mol. Phys. **28**, 5207 (1995).
[20] X. Flechard, S. Duponchel, L. Adoui, A. Cassimi, P. Roncin, and D. Hennecart, J. Phys. B: At. Mol. Phys. **30**, 3697 (1997).
[21] K. Ishii, A. Itoh, and K. Okuno, Phys. Rev. A **70**, 042716 (2004).
[22] M. Hoshino, L. Pichl, Y. Kanai, Y. Nakai, M. Kitajima, M. Kimura, Y. Li, H.-P. Liebermann, R. J. Buenker, H. Tanaka, and Y. Yamazaki, Phys. Rev. A **75**, 012716 (2007).

[23] A. C. K. Leung and T. Kirchner, Phys. Rev. A **93**, 052710 (2016).
[24] R. Ali, P. Beiersdorfer, C. L. Harris, and P. A. Neil, Phys. Rev. A **93**, 012711 (2016).
[25] J.-Y. Chesnel, D. Martina, P. Sobocinski, O. Kamalou, F. Frémont, J. Fernández, and F. Martín, Phys. Rev. A **70**, 010701(R) (2004).
[26] J.-Y. Chesnel, H. Merabet, X. Husson, F. Frémont, D. Lecler, H. Jouin, C. Harel, and N. Stolterfoht, Phys. Rev. A **53**, 2337 (1996).
[27] X. Fléchard, C. Harel, H. Jouin, B. Pons, L. Adoui, F. Frémont, A. Cassimi, and D. Hennecart, J. Phys. B: At. Mol. Phys. **34**, 2759 (2001).
[28] F. Frémont, G. Laurent, J. Rangama, P. Sobocinski, M. Tarisien, L. Adoui, A. Cassimi, J.-Y. Chesnel, X. Fléchard, D. Hennecart, and X. Husson, Int. J. Mol. Sci. **3**, 115 (2002).
[29] M. Schulz, T. Vajnai, and J. A. Brand, Phys. Rev. A **75**, 022717 (2007).
[30] L. Meng, C. O. Reinhold, and R. E. Olson, Phys. Rev. A **42**, 5286 (1990).
[31] W. Wu, J. P. Giese, I. Ben-Itzhak, C. L. Cocke, P. Richard, M. Stockli, R. Ali, H. Schöne, and R. E. Olson, Phys. Rev. A **48**, 3617 (1993).
[32] Z. Chen, C. D. Lin, and N. Toshima, Phys. Rev. A **50**, 511 (1994).
[33] K. Tökésy, Radiat. Phys. Chem. **76**, 621 (2007).
[34] D. Zajfman and D. Maor, Phys. Rev. Lett. **56**, 320 (1986).
[35] M. L. McKenzie and R. E. Olson, Phys. Rev. A **35**, 2863 (1987).
[36] V. J. Montemayor and G. Schiwietz, Phys. Rev. A **40**, 6223 (1989).
[37] J. G. Wang, A. R. Turner, D. L. Cooper, D. R. Schultz, M. J. Rakovic, W. Fritsch, P. C. Stancil, and B. Zygelman, J. Phys. B: At. Mol. Phys. **35**, 3137 (2002).
[38] H. Merabet, G. Cremer, F. Frémont, J.-Y. Chesnel, and N. Stolterfoht, Phys. Rev. A **54**, 372 (1996).
[39] C. L. Kirschbaum and L. Wilets, Phys. Rev. A **21**, 834 (1980).
[40] J. S. Cohen, Phys. Rev. A **51**, 266 (1995).
[41] J. S. Cohen, Phys. Rev. A **54**, 573 (1996).
[42] F. Frémont and A. K. Belyaev, J. Phys. B: At. Mol. Phys. **50**, 045201 (2017).
[43] J. S. Cohen, Phys. Rev. A **56**, 3583 (1997).
[44] R. Abrines and I. Percival, Proc. Phys. Soc. **88**, 861 (1966).
[45] F. Frémont, J. Phys. B: At. Mol. Phys. **49**, 065206 (2016).
[46] L. Liu, J. G. Wang, and R. K. Janev, Phys. Rev. A **89**, 012710 (2014).
[47] A. C. K. Leung and T. Kirchner, Phys. Rev. A **92**, 032712 (2015).
[48] J. Burgdörfer, R. Morgenstern, and A. Niehaus, Nucl. Instrum. Meth. Phys. Res., Sect. B **23**, 120 (1987).
[49] A. Niehaus, J. Phys. B: At. Mol. Phys. **19**, 2925 (1986).
[50] J.-Y. Chesnel, A. Hajaji, R. O. Barrachina, and F. Frémont, Phys. Rev. Lett. **98**, 100403 (2007).
[51] G. Oliviéro, V. Pestel, L. Bottey, M. Philippe, and F. Frémont, Phys. Rev. A **90**, 042711 (2014).